Supporting Information

Nanoroughness, Surface Chemistry and Drug Delivery Control by Atmospheric Plasma Jet on Implantable Devices

Alessandro Patelli,[*,†] Federico Mussano,[‡] Paola Brun,[¶] Tullio Genova,[‡,§] Emmanuele Ambrosi,[‖] Niccoló Michieli,[†] Giovanni Mattei,[†] Paolo Scopece,[⊥] and Lorenzo Moroni[#]

†*Dept. Physics and Astronomy, Padova University, via Marzolo 8, 35131 Padova, Italy*

‡*CIR Dental School, Dept. Surgical Sciences, Torino University, 10126 Torino, Italy*

¶*Dept. Molecular Medicine, Unit of Microbiology, Padova University, 35121 Padova, Italy*

§*Dept. Life Sciences and Systems Biology, Torino University, 10124 Torino, Italy*

‖*Dept. Molecular Sciences and Nanosystems, Venezia University, 30172 Venezia, Italy*

⊥*Nadir srl, 30172 Venezia, Italy*

#*MERLN - Institute for Technology-Inspired Regenerative Medicine, Maastricht University, 6229 ER Maastricht, The Netherlands*

E-mail: alessandro.patelli@unipd.it

Phone: +39 049 827 7039

S1 Samples preparation

S1.1 Surface of the untreated substrates

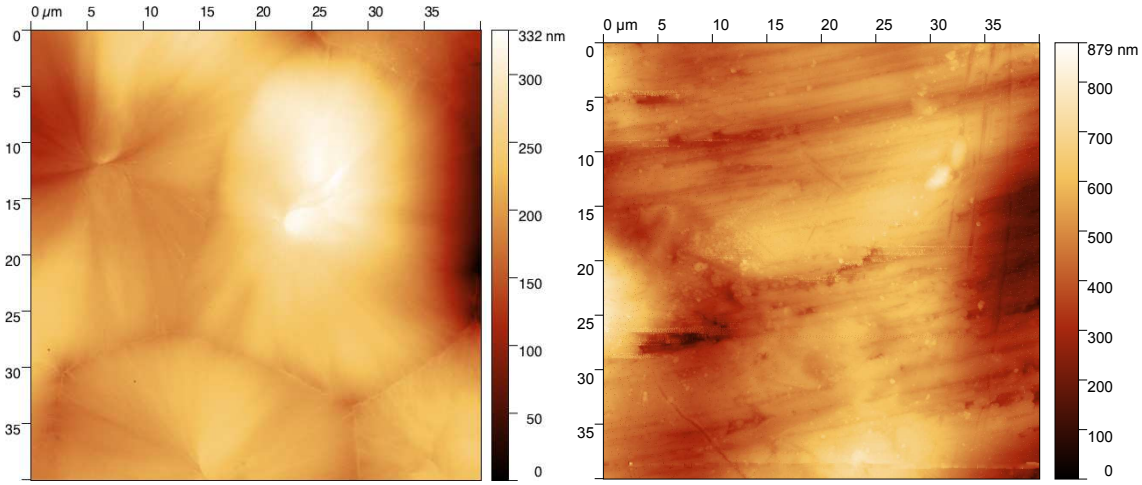

Figure S1: Surface topography of the PCL moulded film (left) and of a T1 substrate (right) measured by AFM in non-contact mode.

S1.2 The atmospheric pressure plasma jet

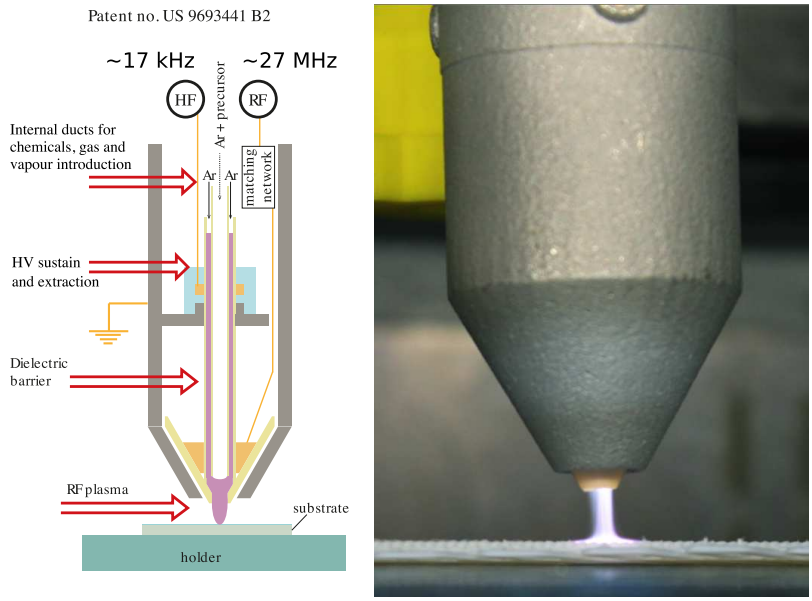

(a) APPJ scheme (b) APPJ photo

Figure S2: (a) Scheme of the novel atmospheric plasma jet (Nadir Stylus Noble). In violet is highlighted the plasma area in the principal alumina tube where Ar process gas is supplied. Externally to this alumina tube are visible the electrodes rings of the HV power supply (∼17kHz) and the RF electrodes (27.12 MHz). Two other ducts are present: an inner capillary for precursors inlet in the vapour or aerosol phase and an outer duct for atmosphere control at the exit of the torch, where air or nitrogen are generally used. The jet works with Ar to avoid energy thermalisation by molecular roto–vibrational motion and by dissociation/recombination reactions, allowing to keep the temperatures of plasma as low as possible. (b) A photograph of the device.

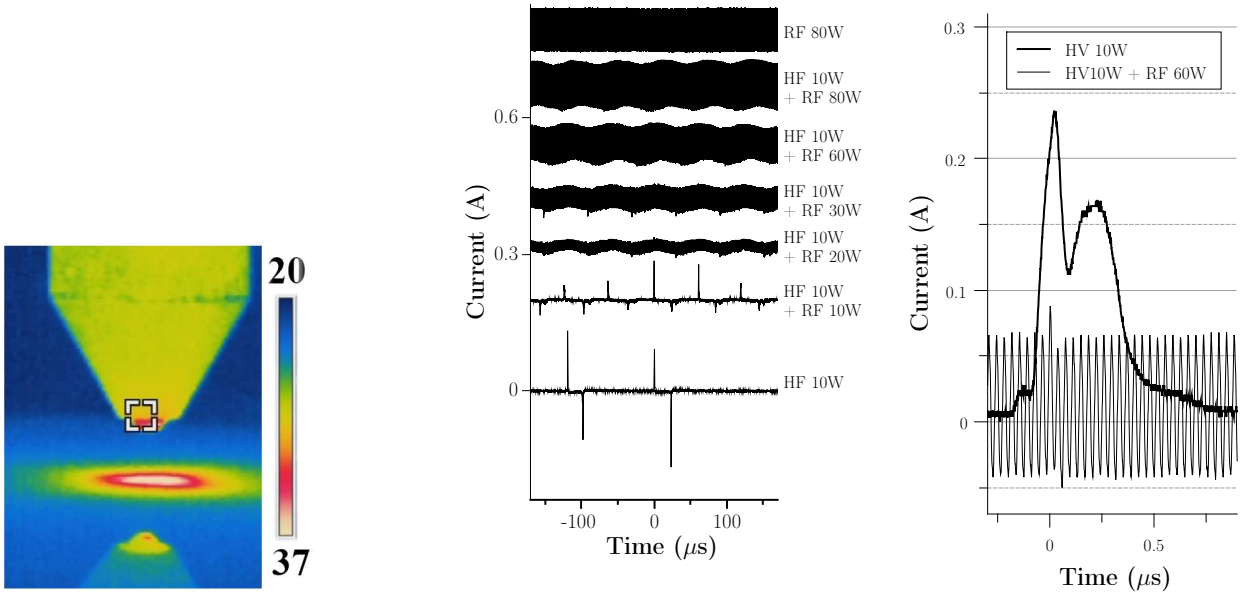

(a) Thermographic image

(b) Current measurement on substrates

Figure S3: a) Image obtained with a thermographic camera of the plasma device on a plastic substrate in stationary conditions (after 5 minutes) and 15W of RF power. The image clearly shows that plasma has no emissions in the infra–red spectral region since it is not thermal. On the substrate the mirrored image of the jet can be observed. b) Electrical characterization on a substrate of the coupling of the HV and RF plasmas, obtained measuring the current on a copper substrate connected to ground with a resistance of 147 Ω. As can be seen by the electrical characterisation, the HV and RF coupling in fact is not just the overlapping of two different plasmas but they also interact with each other. The major effect is that the streamers created by the HV electrodes are blown up by the RF field that rapidly changes the polarity. As a consequence, if hundreds of mA streamers can be measured on a conductive substrate if HV is switched on when both power supplies are active, only a small current bumps of few tens of mA can be measured . In this way local heating is avoided and plasma treatments can be performed at room temperature.

S1.3 The silica nano-particles distribution

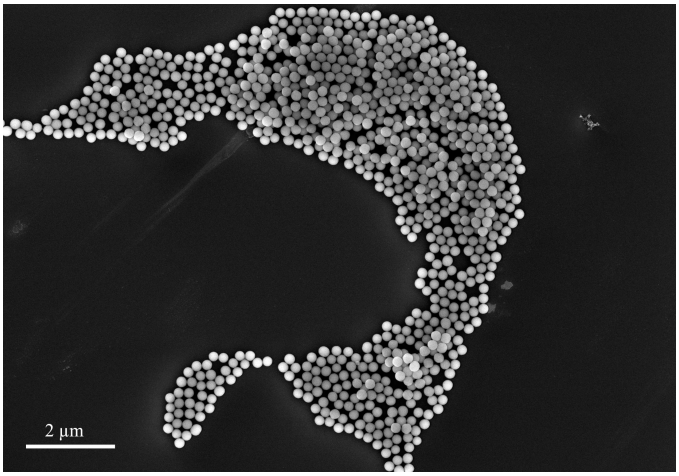

(a) SEM image

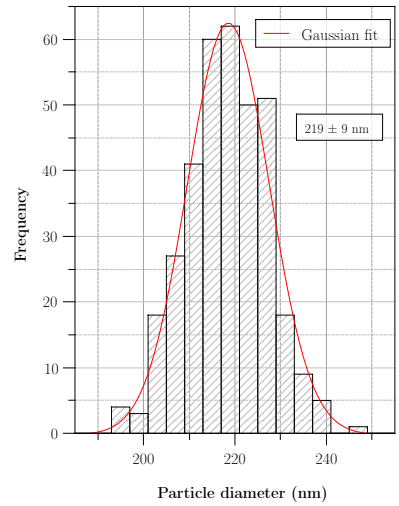

(b) Particles size distribution

Figure S4: (a) SEM image of the SiO_2 nanoparticles produced using the Stöber process deposited on a silicon wafer. (b) Size distribution of the particles derived from the ImageJ (https://imagej.net/Welcome) analysis of the SEM image.

S1.4 Plasma deposition process parameters

Table S1: Process parameters of the plasma jet for the layers deposition. The other parameters are kept constant for all processes: 17 kHz power supply at 8 W, the distance from the samples is 2 mm and the confinement N_2 atmosphere coming from the external duct at 10 slm.

Substrate	**Precursor**	**Ar flux**		**RF**	**pulsing**	**Plotter**
		process	**bubbler**	**power**	**mode**	**speed**
		slm	slm	W	Hz / d.c.	mm/s
Titanium	APTES	4.5	2.5	28	500 / 50%	300
	MMA	4.5	0.5	28	500 / 50%	300
PCL	APTES	4.5	2.5	14	continuous	300
	MMA	4.5	0.2	14	continuous	300

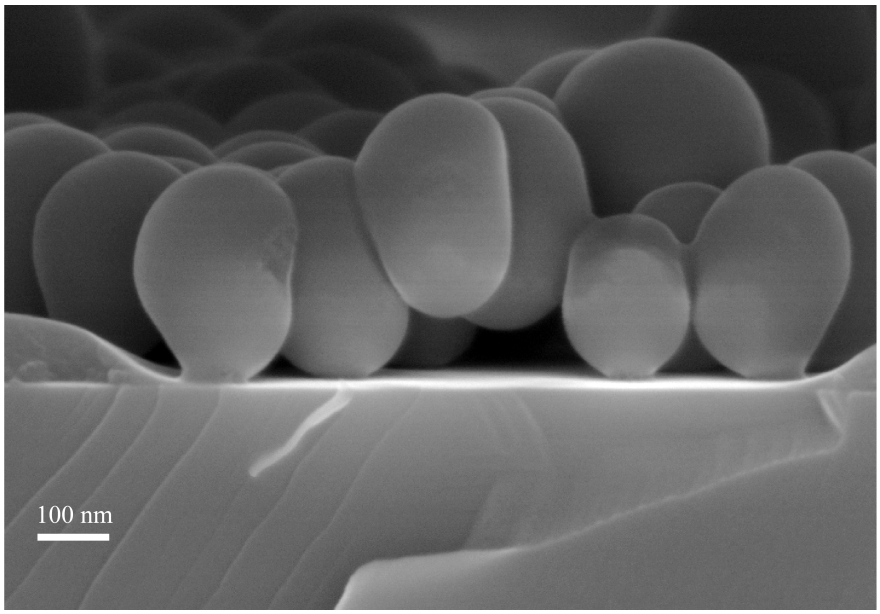

Figure S5: SEM cross section on a nanostructured coating deposited on silicon, where can be highlighted the fixing of the particles to the substrate by the plasma polymer.

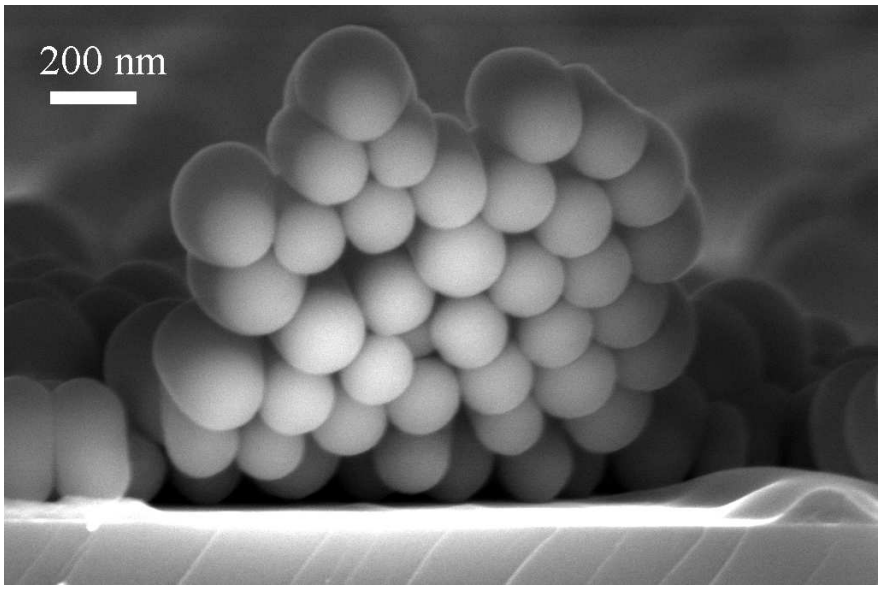

Figure S6: SEM cross section on a nanostructured coating deposited on silicon, where can be highlighted the fixing of the particles among each other by the top plasma polymer.

S1.5 Thermal power load evaluation during APPJ deposition process

The thermal power load (P) on the sample during the APPJ process was obtained by a calorimetry measurement[1,2] using Equation 1,

$$P = mC\frac{d\Delta T}{dt} \tag{1}$$

A copper plate (10×10×2.5 mm^3, mass m = 2.39 mg, specific heat C = 385 mJ g^{-1} $°C^{-1}$) was placed in front of the plasma jet in the same position of the samples treated but in static conditions on a thermally insulated sample-holder. All the parameters was set equal to the ones used in the deposition process. The jet 17 kHz power supply was set at 8 W, RF power supply at 14 W, the distance from the copper plate at 2 mm and the confinement N_2 atmosphere coming from the external duct at 10 slm. The temperature of the copper plate was recorded by a thermocouple put in contact with the surface just after switching off the plasma. The data was taken at different interval of exposure of the copper plate to the plasma. The variation of the temperature ΔT from the room temperature was plotted against the exposures intervals (fig. S7). The copper plate temperature rise up due to the plasma heating until it reaches an equilibrium with thermal losses. The data was fitted with an exponential decay curve and the derivative a time 0 $d\Delta T/dt$ is considered for the calculation in 1.

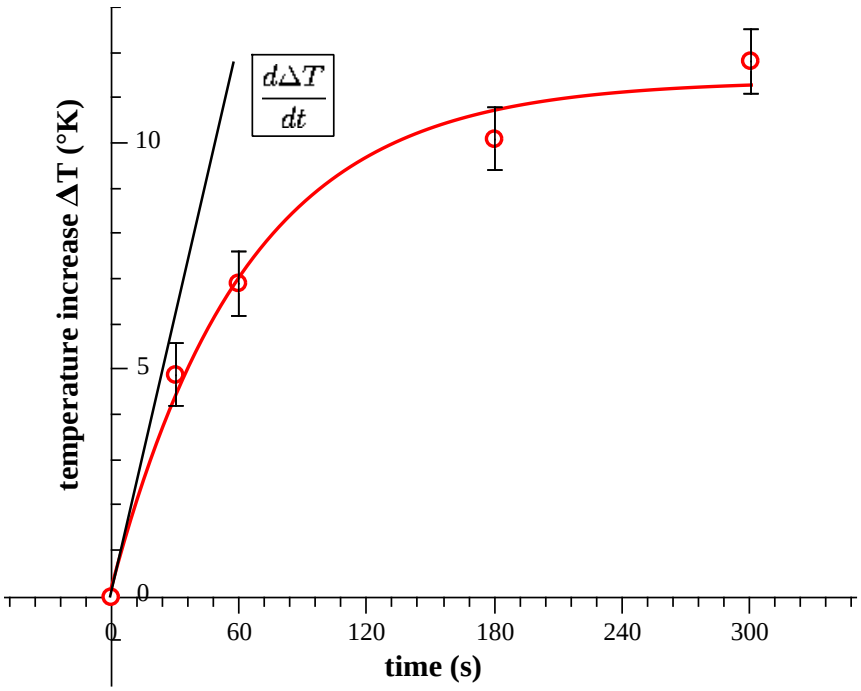

Figure S7: The thermal power load on the sample during the APPJ process was obtained calorimetrically.

S2 Surface morphologies

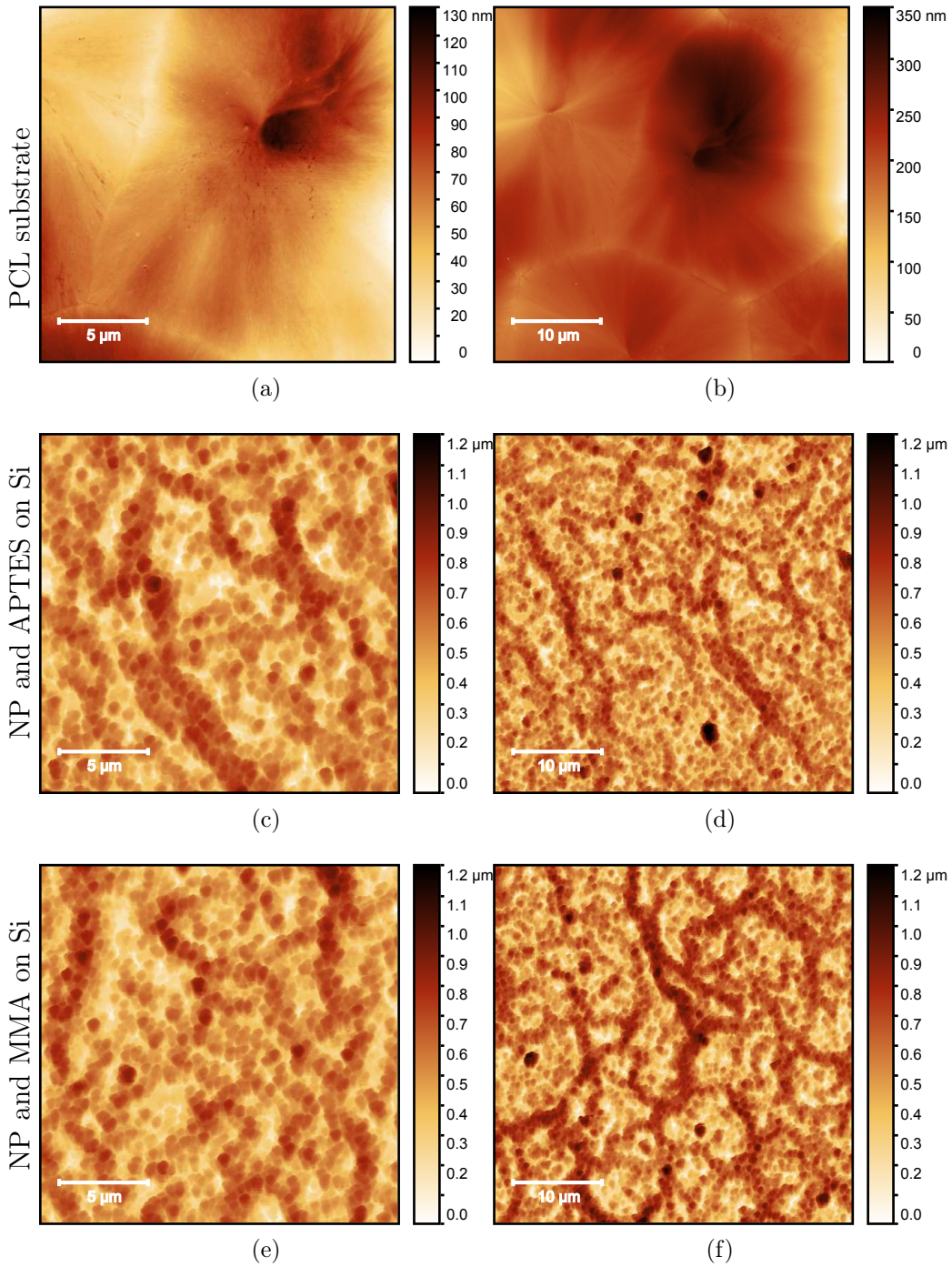

Figure S8: AFM measured topographies on 20×20 μm and 40×40 μm areas for PCL substrate (a,b); APTES plasma polymer coating fixing silica nanoparticles on Si substrate (c,d); MMA plasma polymer coating fixing silica nanoparticles on Si substrate (e,f). Dome size is the combination of the silica particle of ∅ 220 nm and the 100–150 nm coating on top, leading to a size close to 500 nm.

S3 Osteoblasts growth

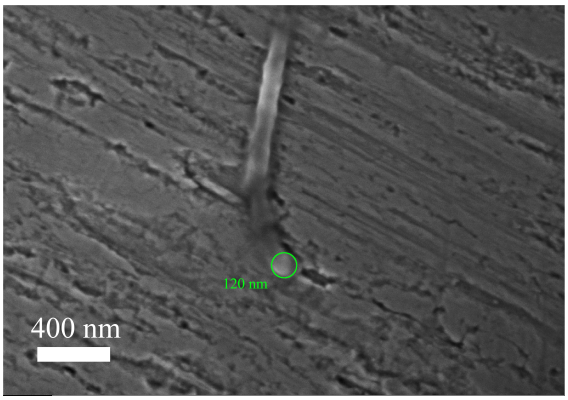

(a) T1 - as worked

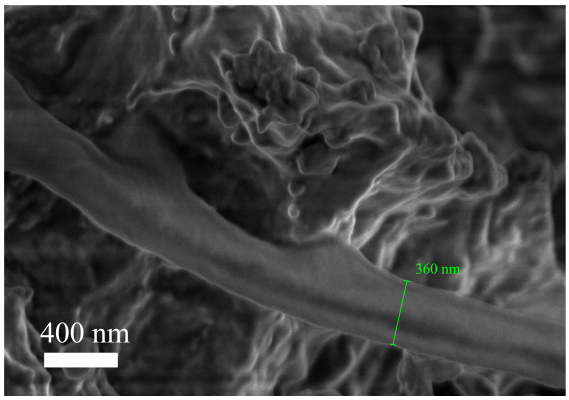

(b) T2 - SBAE

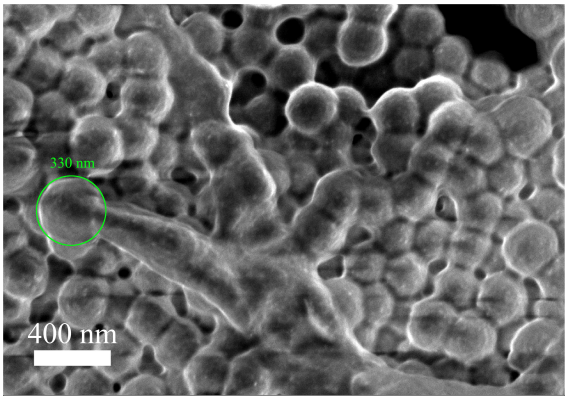

(c) T2 + NP APTES

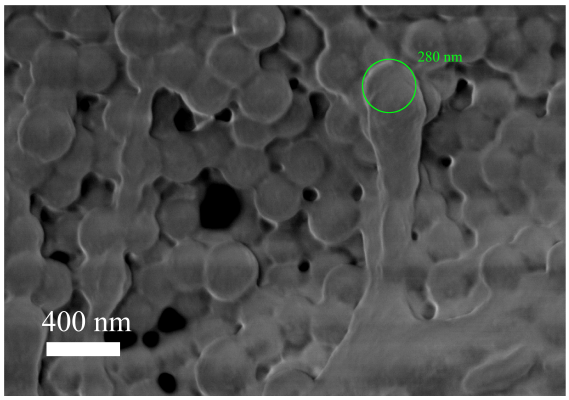

(d) T2 + NP MMA

Figure S9: SEM images highlighting the focal adhesion points of the osteoblasts filipodia on the surfaces (a) on T1 - surface as worked, the filipodia is laying on the surface ; (b) on T2 - SBAE surface, the filipodia is anchoring to microasperities; (c) on T2 with nanoparticles and a fixing plasma polymer starting from APTES precursor, the filipodia are so adherent to the substrate that are merely recognised; (d) T2 with nanoparticles and plasma polymer starting from MMA precursor, as in (c) the filipodia are difficult to detect and focal adhesion points have the same size of the nanoparticles.

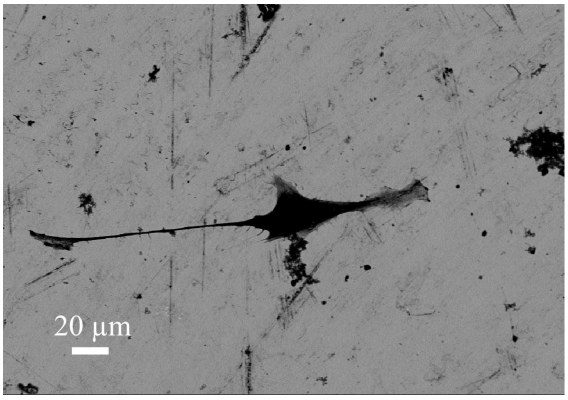

(a) T1 - as worked

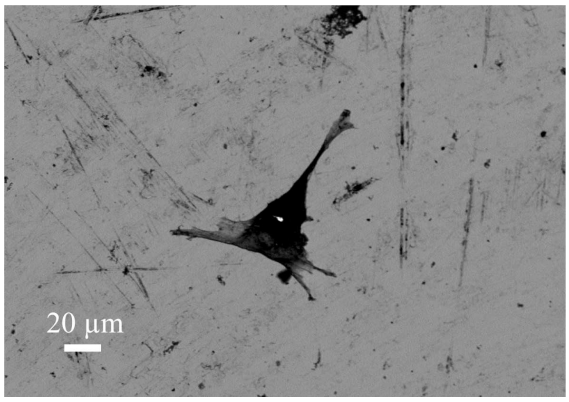

(b) T1 - as worked

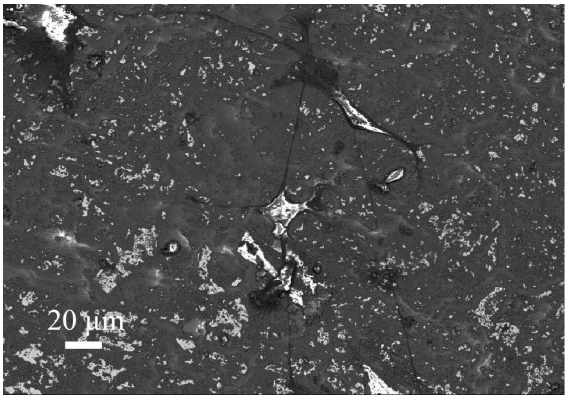

(c) T1 + NP APTES

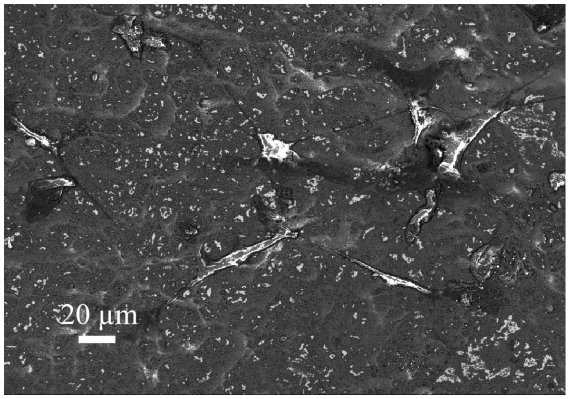

(d) T1 + NP APTES

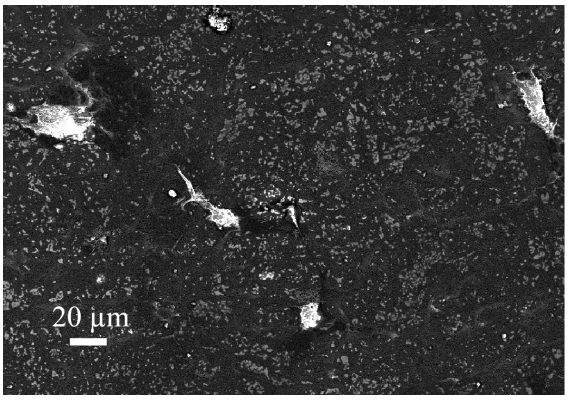

(e) T1 + NP MMA

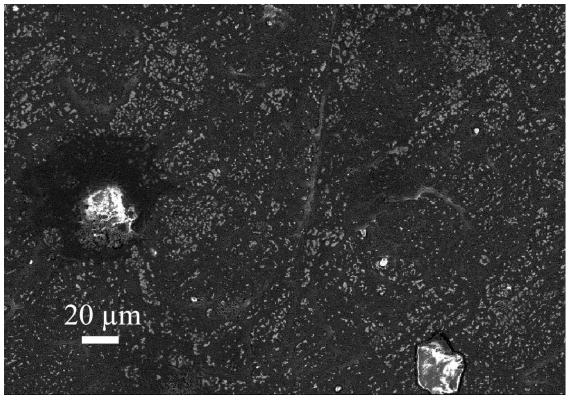

(f) T1 + NP MMA

Figure S10: SEM images of cells morphology with the Backscattering detector on T1 - as worked substrate: (a,b) T1 as is; (c,d) T1 with silica nanoparticles and fixing plasma polymer starting from APTES precursor; (e,f) T1 with silica nanoparticles and fixing plasma polymer starting from MMA precursor.

S4 Fibroblasts growth

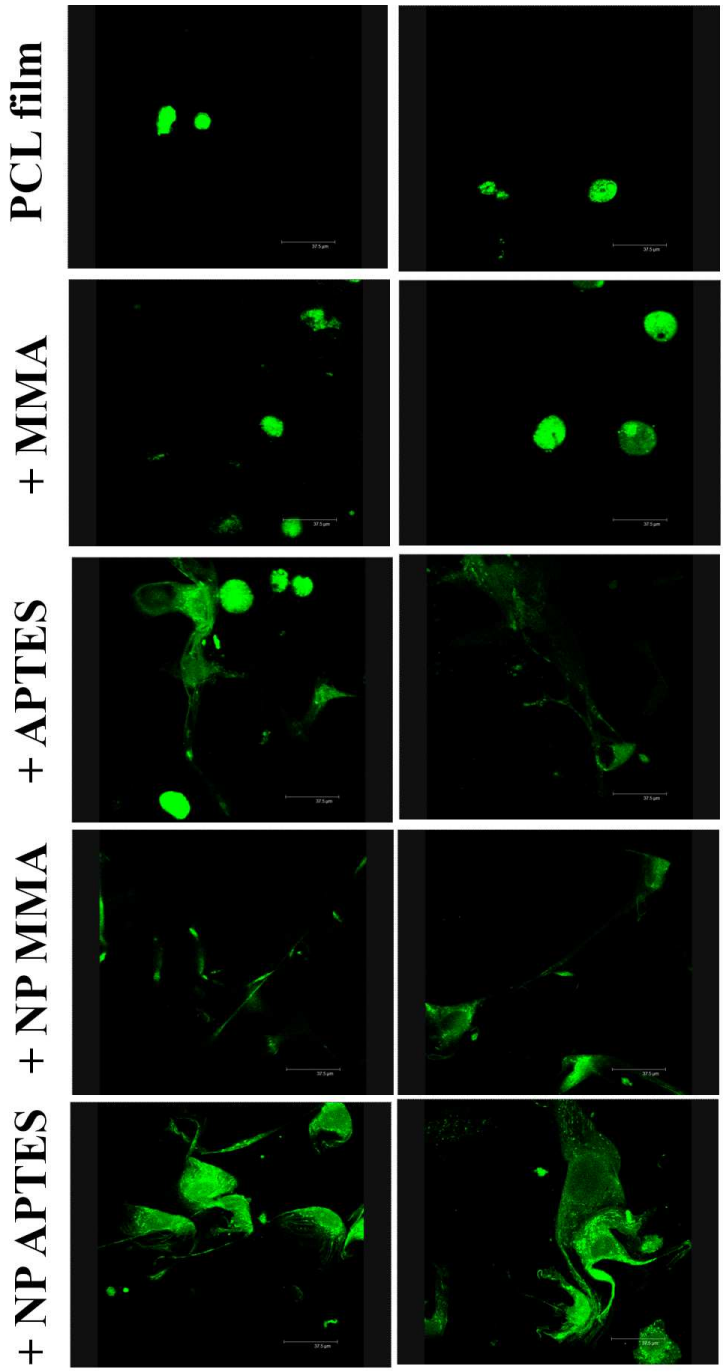

Figure S11: Cell proliferation assays - confocal microscopy: cells were labelled with CFSE cell tracer (Carboxyfluorescein succinimidyl ester; ThermoFisher), a green fluorescent dye retained within cells for long periods. Once incorporated within cells the dye is not transferred to adjacent cells but it halves within daughter cells thus following each cell division up to 7-8 divisions. Cells were fixed and CFSE-related green fluorescent signal was observed at confocal microscopy).

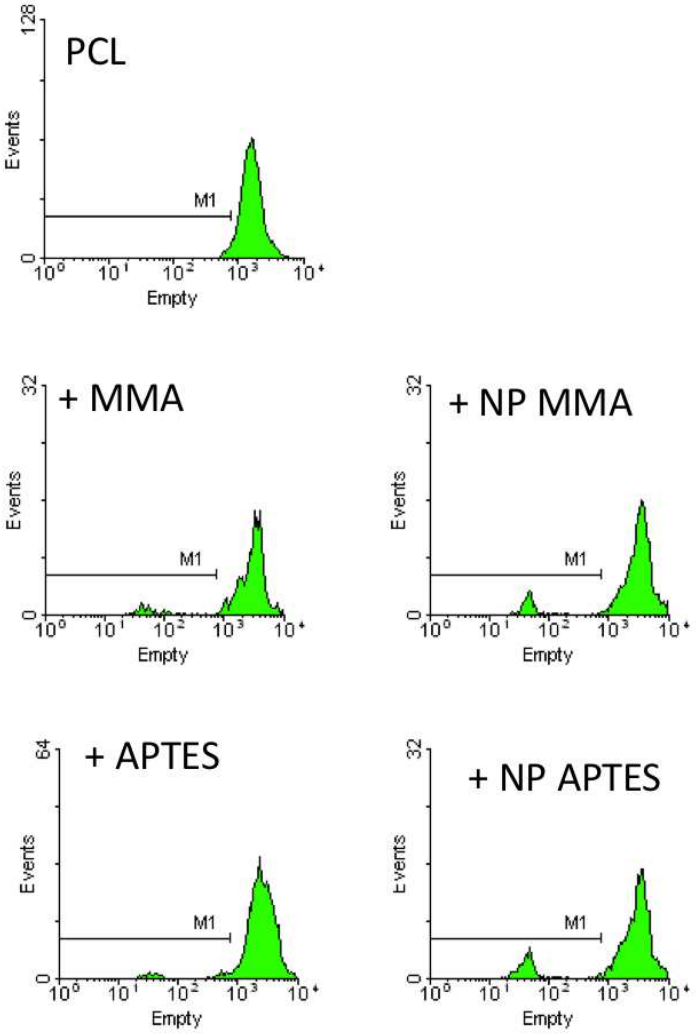

Figure S12: Cell proliferation assays - flow cytometry: cells were labelled with CFSE cell tracer (Carboxyfluorescein succinimidyl ester; ThermoFisher),a green fluorescent dye retained within cells for long periods. Once incorporated within cells the dye is not transferred to adjacent cells but it halves within daughter cells thus following each cell division up to 7-8 divisions. Percentage of positive cells were quantified by FACS analysis.

S5 Fluorophore release

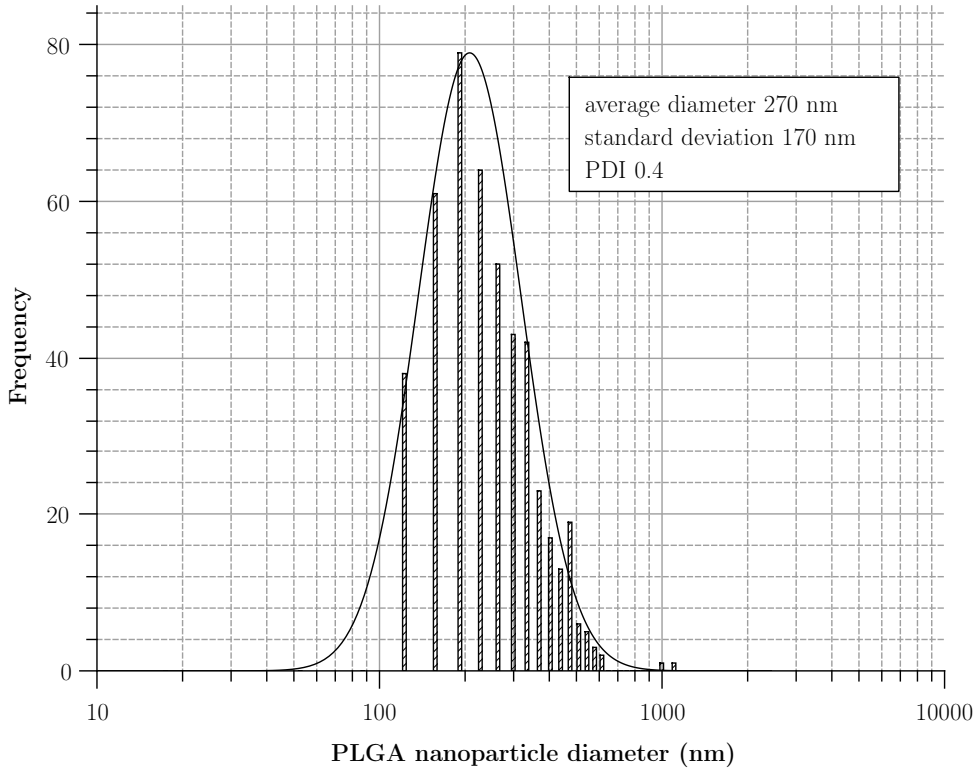

Figure S13: Size distribution of PLGA DEGRADEX® particles with an embedded fluorophore derived from the ImageJ (https://imagej.net/Welcome) analysis of the a image. The distribution is similar to the one measured by the supplier https://www.sigmaaldrich.com/technical-documents/articles/technology-spotlights/degradex-microspheres-nanoparticles.html

References

(1) DIN EN 60601-1-6:2010: Medical electrical equipment (IEC 60601-1-6:2010). 2015.

(2) Foest, R.; Kindel, E.; Lange, H.; Ohl, A.; Stieber, M.; Weltmann, K.-D. RF Capillary Jet - a Tool for Localized Surface Treatment. *Contributions to Plasma Physics* **2007**, *47*, 119–128.